Viability of FASER as a Delivery Gilder using Wind Tunnel Tests to Characterize Center of Gravity, Payload, and Stability Limits while Maximizing Glide Distance

Trevor Burgoyne, AEM 4303W

3 April 2023

Abstract

This report details the experiments performed using an UltraStick-120 airframe (also known as FASER) in a Closed Return wind tunnel, and the subsequent analysis performed to characterize the stability of said airframe in order to provide relevant performance limitations for its potential use as a delivery glider. The longitudinal stability of the FASER aircraft is investigated by collecting wind tunnel data for a range of elevator deflections and angles of attack. The forward and aft limits of the location of the center of gravity are determined for flight conditions that maximize glide distance. The center of gravity limits are found to be at 5.17 cm and 9.8 cm behind the leading edge of the wing, assuming an allowable elevator deflection of ± 15°. A maximum payload of 478.5 N and a minimum flight speed of 13 m/s are also found to be within the stability limits. Further investigation into FASER's capabilities and limitations as a glider is recommended to build upon the results presented.

Introduction

In places where a full-sized aircraft cannot land, using gliders to deliver emergency supplies is being considered as a viable alternative. Companies such as Zipline have explored using a wide variety of aircraft designs and approaches to solve similar delivery problems, but are more generally geared towards operation in populated areas [1]. For more remote scenarios where large warehouse and docking infrastructure may be impractical, a glider could be deployed from a powered aircraft at an appropriate altitude and then undertake an unpowered glide to gracefully approach its destination. A promising candidate for such a glider is the Free-flying Aircraft for Sub-scale Experimental Research (FASER), also known as the UltraStick-120, which has been used by NASA's Langley Research Center for flight research [2]. To verify its potential utility as a glider carrying a payload from as high as 20,000 ft, wind tunnel tests were conducted to determine FASER's longitudinal equations of motion. This includes determining the forward and aft center of gravity limits, as well as the minimum speed and maximum payload for which it can be trimmed to fly at those limits. To enable the widest possible range of applications, all these limits were determined with maximizing the glide distance in mind. While it may not always be the case, having the capability to glide into a delivery site from as far away as possible would be advantageous, since it would require the powered aircraft carrying the glider to travel less distance and would help it avoid any potentially dangerous operational areas.

Apparatus & Methodology

The experiment was performed using a mini-Ultrastick model airplane (FASER) in the Closed Return (CR) wind tunnel in Akerman Hall at the University of Minnesota-Twin Cities. The aircraft was mounted to a sting that could pitch up and down to adjust the

angle of attack (see Figure 1 in the Appendix). The angle of attack, as well as the axial and normal forces, were measured by the sting during the experiment and automatically recorded using a lab computer. The same computer received air data, such as air speed and pressure, reported from a pitot tube mounted inside the tunnel. The variables changed during the experiment were the angle of attack (from -10° to 22° at 2° increments) and the elevator deflection, which was limited to three distinct positions (18°, 0°, and -18°) for each angle of attack.

Before collecting data, the force sting was tared so as to not include the weight of FASER itself in the forces recorded. Then to begin, the angle of attack was set to -10°, with the elevators at zero deflection. The wind tunnel was brought up to a freestream velocity of about 8 m/s, at which point the data collection software was run to collect air and sting data. Once data was collected, the elevator was then adjusted to a deflection of 18°, data was again collected, and then adjusted once more to a deflection of -18°, all at the same angle of attack. After all three elevator deflections were recorded, the wind tunnel was turned off and the process was repeated again for the next angle of attack, increasing at 2° increments until 22°. Care was taken to tare the sting after each angle of attack adjustment to ensure valid force readings.

To simplify calculations, and because the aircraft spanned nearly the whole width of the tunnel, all 3D effects are ignored in this analysis. Because the freestream velocity was always well below Mach 0.3, the flow will also be considered to be incompressible, allowing for more confidence in our pitot measurements, which are in part dependent on Bernoulli's equation, which is only valid for incompressible flows. Additionally, the experimental air temperature, density, and dynamic viscosity will be taken as constant, since the tunnel can be considered a closed system and experienced very little variation over the course of the experiment.

Methods

From the recorded sting data, C_L, C_M, and C_D will be calculated using the general formulas for such coefficients:

$$q = \frac{1}{2}\rho v^2 \quad C_D = \frac{D}{qS} \quad C_L = \frac{L}{qS} \quad C_M = \frac{M}{qSc} \tag{1}$$

where q, or dynamic pressure, is a function of the density ρ and the freestream velocity v. In the numerator for each coefficient are the drag force D, lift force L, and total moment M, and in the denominator the wing area S and the chord length c.

In Figures 2 and 3 in the Appendix, the geometry of the test aircraft is illustrated. Due to the different frames of reference between the sting measurements and the aircraft body, the lift and drag forces will be computed as follows:

$$D = -X\cos(\alpha) - Z\sin(\alpha) \qquad L = X\sin(\alpha) - Z\cos(\alpha) \tag{2}$$

where α is the angle of attack, and X and Z are the forces measured by the sting in the horizontal and vertical directions, respectively.

The analysis of the longitudinal stability of the aircraft will start by determining the experimental location of the neutral point as follows:

$$np = cg - \frac{\delta C_M}{\delta C_L} \qquad SM = -\frac{\delta C_M}{\delta C_L} \tag{3}$$

where np and cg are, respectively, the chord-normalized locations of the neutral point and center of gravity measured from the leading edge of the wing, and $\frac{\delta C_M}{\delta C_L}$ is the slope of the C_M vs C_L curve, which is also equal to the negative of the static margin (SM). Once the neutral point is identified using the known experimental location of the center of gravity, the forward and aft limits of the center of gravity will be determined by computing the minimum and maximum $\frac{\delta C_M}{\delta C_L}$ that will still allow the aircraft to be trimmed at the necessary C_L.

Lastly, in this analysis all values will be computed such that the glide distance will be maximized. From theory, the maximum glide distance is achieved with the lift-to-drag ratio is maximized, which occurs when

$$K = \frac{1}{\pi ARe} \qquad C_{D0} = C_D - KC_L^2 \qquad C_{L,glide} = \sqrt{\frac{C_{D0}}{K}} \tag{4}$$

where C_{D0} is the parasite drag coefficient, AR is the wing aspect ratio, and e is the oswald efficiency factor, which is approximated as

$$e = 1.78[1 - .045AR^{.68}] - .64 \tag{5}$$

This analysis will use the lift coefficient required to achieve maximum glide, $C_{L,glide}$, as the desired C_L for the aft and forward limits of the center of gravity, and thus will provide the range of center of gravity locations for which $C_{L,glide}$ is trimmable.

During the wind tunnel testing, wind tunnel conditions were constant, save for small variations as the tunnel was brought down and back up to speed while the angle of attack was adjusted. A summary of the average experimental conditions is presented in Table 1.

Air Density (kg/m^3)	Air speed (m/s)	Chord Length (m)	Wing Area (m^2)
1.169	8.477	0.2129	0.2007

Table 1: Average experimental conditions for all wind tunnel tests, as measured by a pitot tube and reported through a lab computer. Additionally, the chord length and wing area of the test aircraft.

Results

From the data collected from both the sting and the air data sensors at various angles of attack, C_L, C_M, and C_D were all calculated in MATLAB and are shown in Figures 4-6 for each of the three elevator deflections. The selection of the angles of attack was motivated by a desire to capture a large region of linear correlation between C_L and α, as this is the region of interest for the overall analysis of longitudinal stability. As stall behavior is outside of the scope of this analysis, all calculations are done using only data from before stall (from Figure 6, stall is at about α = 14°, where the linear relationship breaks down).

In Figure 4, the relationship between C_M and C_L is presented for each of the three elevator deflections tested. Since the location of the neutral point and center of gravity were constant throughout the experiment, equation (3) indicates that the slope of the C_M vs C_L curve will be constant regardless of elevator deflection, which is exactly what can be seen in Figure 4. What does change with elevator deflection is the location of the y-intercept of each curve, which decreases as elevator deflection increases. The trailing ends of the otherwise linear trends observed in the data are a result of stall conditions and are not considered in this analysis and subsequent calculations.

In Figure 5, the coefficients of drag and lift are shown, and once again a clear increase in drag occurs at high C_L as stall conditions set in and flow separates from the lifting surface. The drag data will be used in tandem with equation (4) to help determine the optimal C_L for maximum glide, and the details of those calculations are presented in the Appendix.

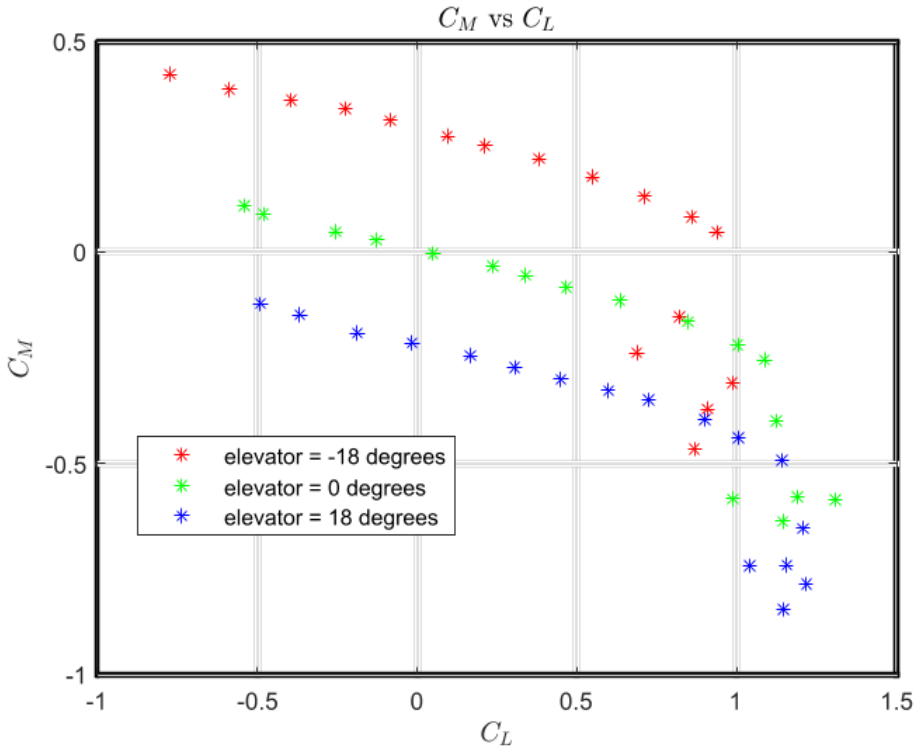

Figure 4: Plot of C_M versus C_L for all three elevator angles. Note that the y-intercept for 18° is negative, and at 0° the intercept is approximately zero.

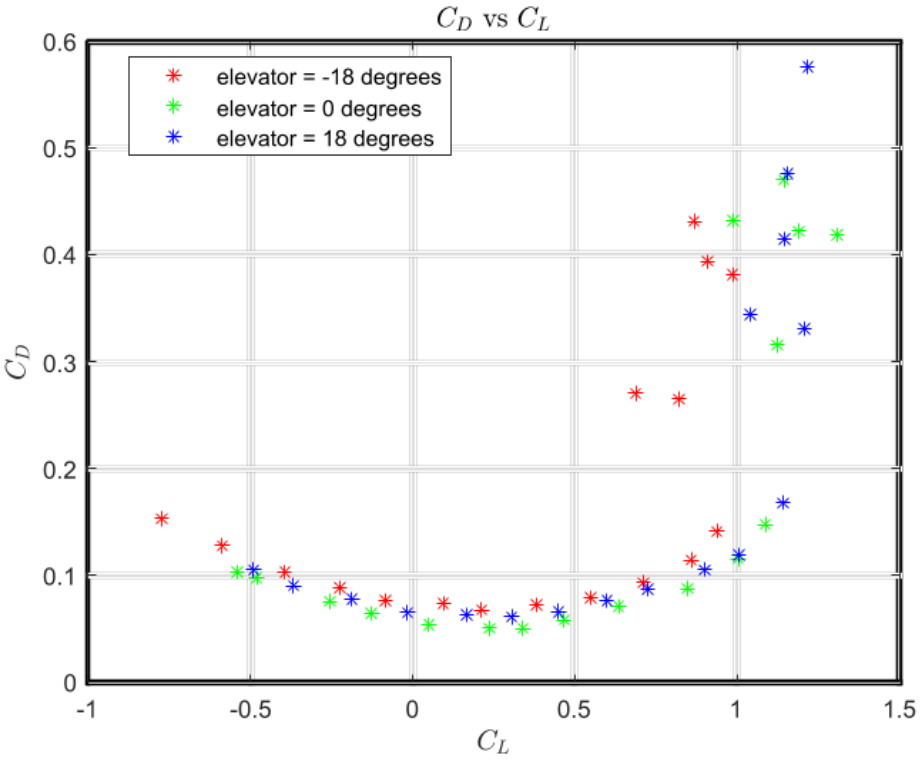

Figure 5: Plot of C_D versus C_L for all three elevator angles.

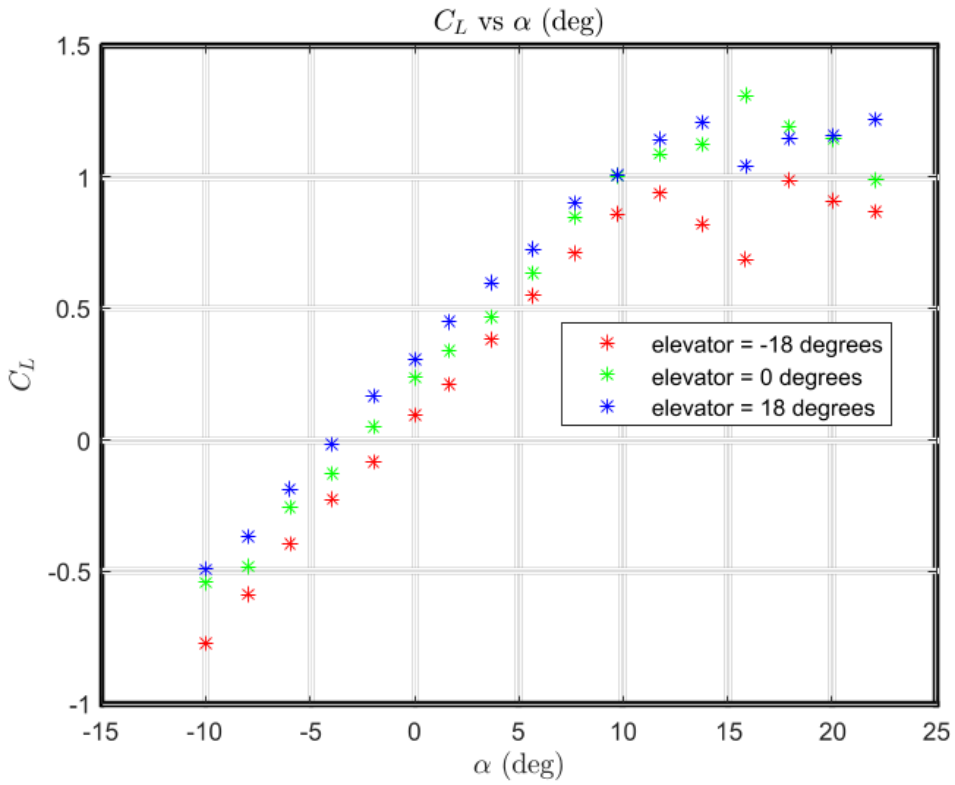

Figure 6: Plot of C_L versus α for all three elevator angles. Note that the linear region before stall (α ~= 14°) has an almost identical slope for all three deflections.

In Figure 6 we observe a clean, linear trend of increasing C_L as *α* increases, as expected from airfoil theory. The effect that elevator deflection has on the slope of this curve is very minimal, and mostly just serves to shift the curve up or down. In Figure 4, it can be seen that while all three elevator deflections give rise to negative slopes (a requirement for static stability), they do not all have a positive y-intercept. The fact that the highest elevator deflection of 18° has a negative intercept while the others do indicates that the aft-most limit for the location of the center of gravity will be at the neutral point, which is discussed in greater detail in the General Discussion section.

For conservativeness in design, the analysis will restrict the available maximum elevator deflection on the aircraft to ± 15°, which ensures that there will be ample elevator deflection available to achieve longitudinal stability, even at the extreme aft and forward limits of the location of the center of gravity. Additionally, the maximum speed at which elevator flutter sets in is taken as 45 m/s, and the minimum speed of FASER is 8 m/s [2].

Using the coefficients described, the aerodynamic and stability coefficients are calculated and shown in Table 2.

Elevator Deflection (°)	Static Margin	C_L vs α slope (deg^{-1})	Pitch Stiffness (deg^{-1})	x_{np} / c	h_{np} / c	Elevator Power (deg^{-1})
18	-0.1902	0.0767	-0.0162	0.4601	0.165	-0.0138
0	0.0033	0.0787	-0.0165	0.4598	0.165	-0.0138
-18	0.2998	0.0801	-0.0170	0.4609	0.165	-0.0138

Table 2: Stability coefficient estimates for each measured elevator deflection.

The C_L vs α slope was determined by using a linear fit of the C_L vs α curve before stall, and similarly pitch stiffness was found from a linear fit of the C_M vs α curve before stall. The Elevator Power is simply a linear fit of C_M at zero C_L vs the elevator deflection, which yields a metric for how much elevator deflection affects C_M. By using the calculated Elevator Power, a similar table can be generated for our decided limits of ± 15° deflection, which results in the following:

Elevator Deflection (°)	Static Margin	Pitch Stiffness (deg^{-1})
15	-0.1538	-0.0162
-15	0.2555	-0.0170

Table 3: Aerodynamic and stability coefficient estimates for the conservative limits of elevator deflection, ± 15°.

The C_L that maximizes the glide distance can be computed using the parasitic drag coefficient, wing aspect ratio, and the oswald efficiency ratio as shown in equation (5). The aspect ratio and oswald efficiency ratio are functions of the geometric properties of FASER. The aspect ratio used in this report is taken from [2] to be 4.778, which in turn yields an oswald efficiency factor of 0.908. The overall parasitic drag coefficient is computed as the average parasitic drag coefficient of each elevator deflection and angle of attack, with the details of the calculation found in the Appendix. The results of these computations are presented in Table 4.

AR	e (oswald efficiency)	Parasitic Drag Coefficient	$C_{L,glide}$
4.778	0.908	0.089	1.101

Table 4: Intermediate and final values from the computation of the C_L that maximizes glide distance.

General Discussion

The theoretical aft limit for the location of the center of gravity of any aircraft will be at its neutral point, which corresponds to neutral stability and a static margin of zero. In order for this to be actually feasible, there has to be an achievable elevator deflection such that the y-intercept of the C_M vs C_L curve is zero, since this will yield a C_M of zero for any C_L. Such a deflection is guaranteed to exist so long as one of the limits of allowable elevator deflections has a negative static margin, which happens to be true in this case (from Table 3, the Static Margin at 15° deflection is indeed negative). Therefore the aft limit of the FASER's center of gravity is in fact at its neutral point. From Table 2, the average location of the neutral point is at 0.4603 (chord normalized), or about 9.8 cm behind the leading edge of the wing.

The theoretical forward limit for the location of the center of gravity is the very front of the aircraft, which in practice is not feasible if stability is desired. This is because as the center of gravity moves forward, the static margin increases, which in turn means that the C_L required to trim the aircraft decreases. In graphical terms, this is because the x-intercept of the C_M vs C_L curve will decrease as the magnitude of the slope increases. Thus the forward position of the center of gravity is limited by the $C_{L,glide}$ necessary to glide FASER the desired maximum distance (from Table 3) as well as the lowest elevator deflection we can achieve, which is -15°. With these limitations, the actual forward limit of the center of gravity is 0.2427 (chord normalized), or about 5.17 cm behind the leading edge of the wing.

Since both the forward and aft limits are based on the same $C_{L,glide}$ for maximum glide distance, both cases will have the same minimum necessary speed to maintain the trim state at that C_L. Rearranging the formula for C_L in equation (1), we can get an expression for this minimum trim velocity:

$$v_{min}^2 = \frac{2W_{min}}{\rho_{max} C_{L,glide} S} \quad (6)$$

where W_{min} is the minimum weight and ρ_{max} is the maximum air density during flight. From [2] the weight of FASER on its own is 19.72 lbf (87.72 N), and for normal flight conditions the maximum air density we could expect would be at sea level (1.225 kg/m^3). Using these values, the minimum trim velocity would be 13 m/s.

Since the whole point of this investigation was to determine FASER's suitability as a delivery glider, it is fair to question how much additional weight FASER can actually carry. Given that elevator flutter sets in at 45 m/s, this limits the maximum allowable weight for FASER. By once again rearranging equation (7), we can solve for this maximum weight limit:

$$W_{max} = \frac{1}{2}\rho_{min} v_{max}^2 C_{L,glide} S \tag{7}$$

where now ρ_{min} is the air density at the altitude considered for the mission start, or 20,000 ft (6096 m) which has a density of about 0.6601 kg/m^3. Thus assuming top speed and a C_L that maximizes glide distance, the max weight that can be carried for either the forward or aft limit is 566.2 N. Subtracting the weight of FASER itself, this leaves a maximum payload of 478.5 N. A summary of these limits is presented in Table 5.

	Forward Limit	Aft Limit
Location of Center of Gravity (cm from leading edge)	5.17	9.8
Minimum Speed to Trim (m/s)	13	13
Maximum Payload (N)	478.5	478.5

Table 5: Center of gravity limits for maximum glide distance flight conditions.

Conclusion

The wind tunnel experiment described here aimed to characterize the longitudinal stability of the FASER aircraft and determine the forward and aft limits of the location of the center of gravity during a flight that maximizes glide distance. By using measurements taken within a Closed Return wind tunnel using a force sting and pitot tube, coefficients of lift, drag, and moment were calculated for a range of elevator deflections and angles of attack. From the analysis of these aerodynamic coefficients,

the center of gravity limits were found to be at 5.17 cm and 9.8 cm behind the leading edge of the wing in order for the aircraft to be statically stable within ± 15° elevator deflection and at the $C_{L,glide}$ that results in the maximum glide distance. The maximum payload that FASER could carry at either of these limits was found to be 478.5 N, and the minimum speed needed to trim the aircraft when carrying no payload is 13 m/s. This provides key insight into how a potential FASER delivery glider would need to be loaded up with its payload, and provides a reasonable safety envelope of the additional ± 3° elevator deflection that could be used to further ensure the aircraft stays trimmed during flight. Further investigation could be made into how FASER performs in actual glide conditions, and how well automatic or pilot-operated control systems can maintain stability during flight, which may highlight additional restrictions to where the center of gravity location may lie. Additionally, further analysis could be made with the same data collected here to characterize center of gravity limits under different conditions (ie, where maximum glide is not required). Further exploration could also test FASER at a wider range of elevator deflections to more fully and accurately characterize its performance, since time restraints limited such detail in this report.

References

[1] Kolodny & Brigham. “Zipline unveils P2 delivery drones that dock and recharge autonomously.” *CNBC*, 15 Mar. 2023, https://www.cnbc.com/2023/03/15/zipline-unveils-p2-delivery-drones-that-dock-and-recharge-autonomously.html. Accessed 30 Mar. 2023.

[2] Owens, D., Cox, D. and Morelli, E., “Development of a Low-Cost Sub-Scale Aircraft for Flight Research: The FASER Project,“ AIAA 2006-3307, 25th AIAA Aerodynamic Measurement Technology and Ground Testing Conference, June 2006. https://doi.org/10.2514/6.2006-3306

Appendix

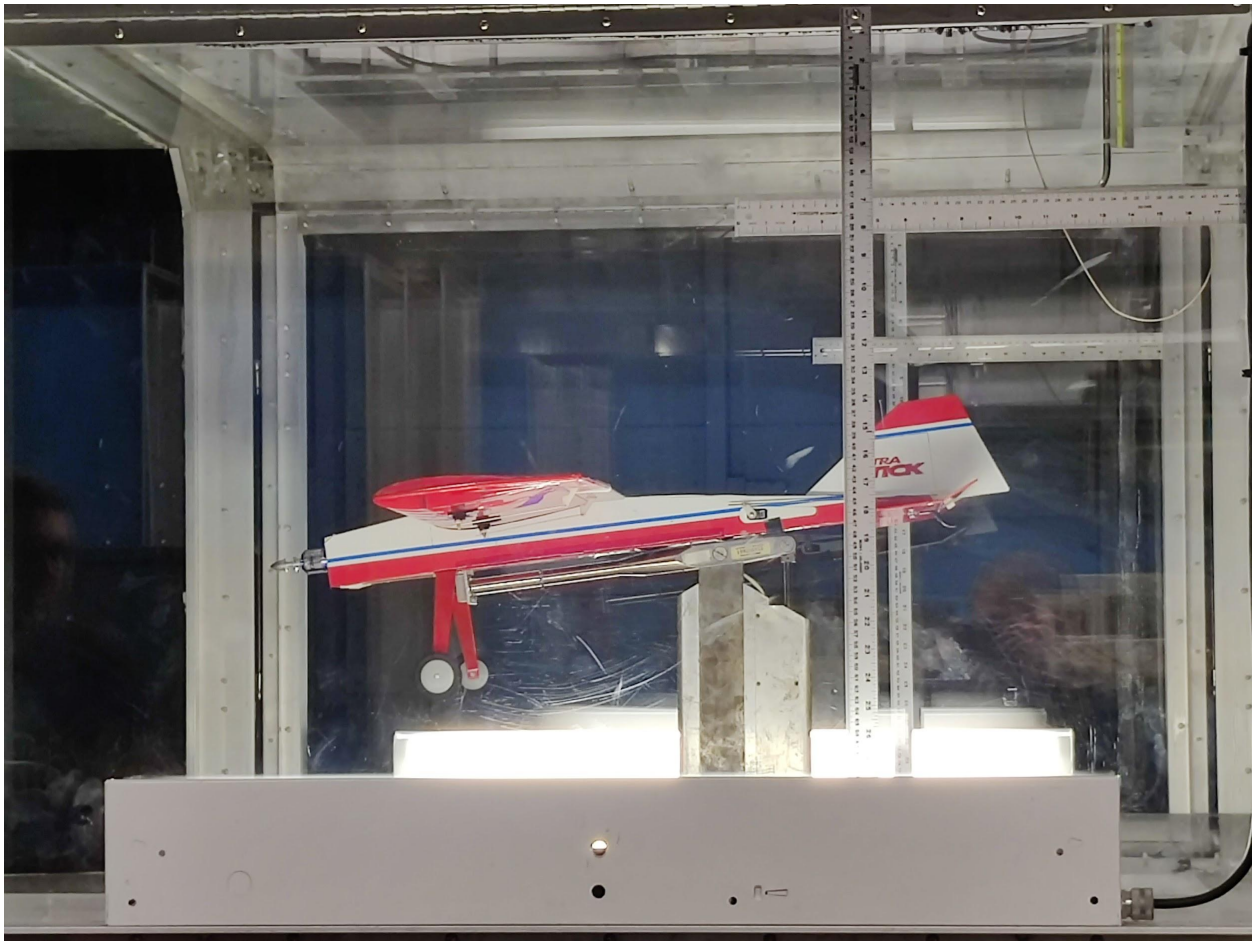

Figure 1: The mini-Ultrastick model aircraft, aka FASER, mounted to the sting in the Closed Return wind tunnel in Akerman Hall at the University of Minnesota. Photo credit: Trevor Burgoyne.

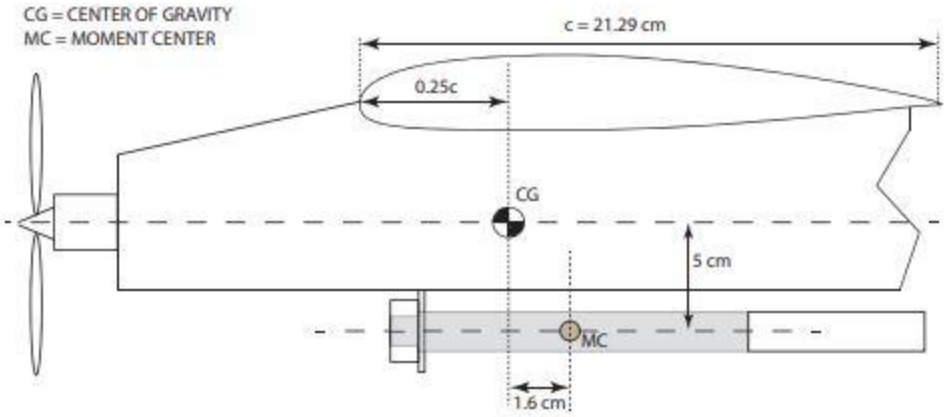

Figure 2: Geometry of the FASER-sting system, with the center of gravity of the aircraft and the moment center of the string clearly labeled. Figure credit: "Wind Tunnel Lab Manual," Demoz Gebre-Egziabher.

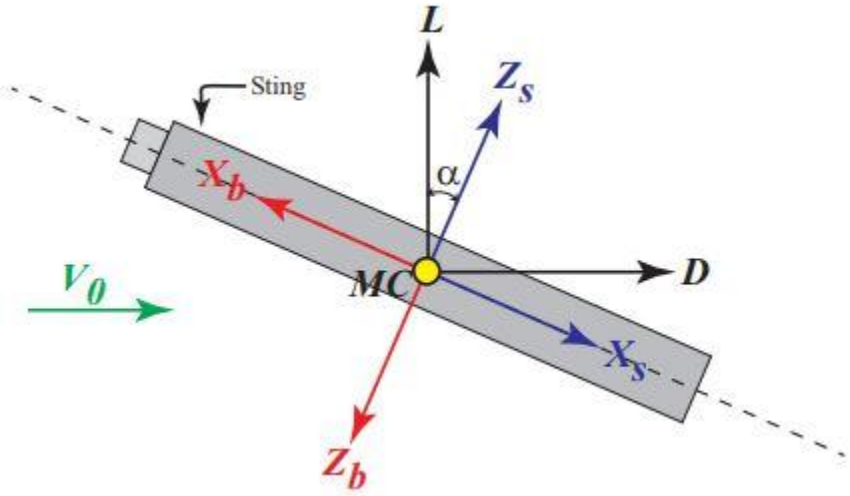

Figure 3: Coordinate system of the wind tunnel sting. Figure credit: "Wind Tunnel Lab Manual," Demoz Gebre-Egziabher.

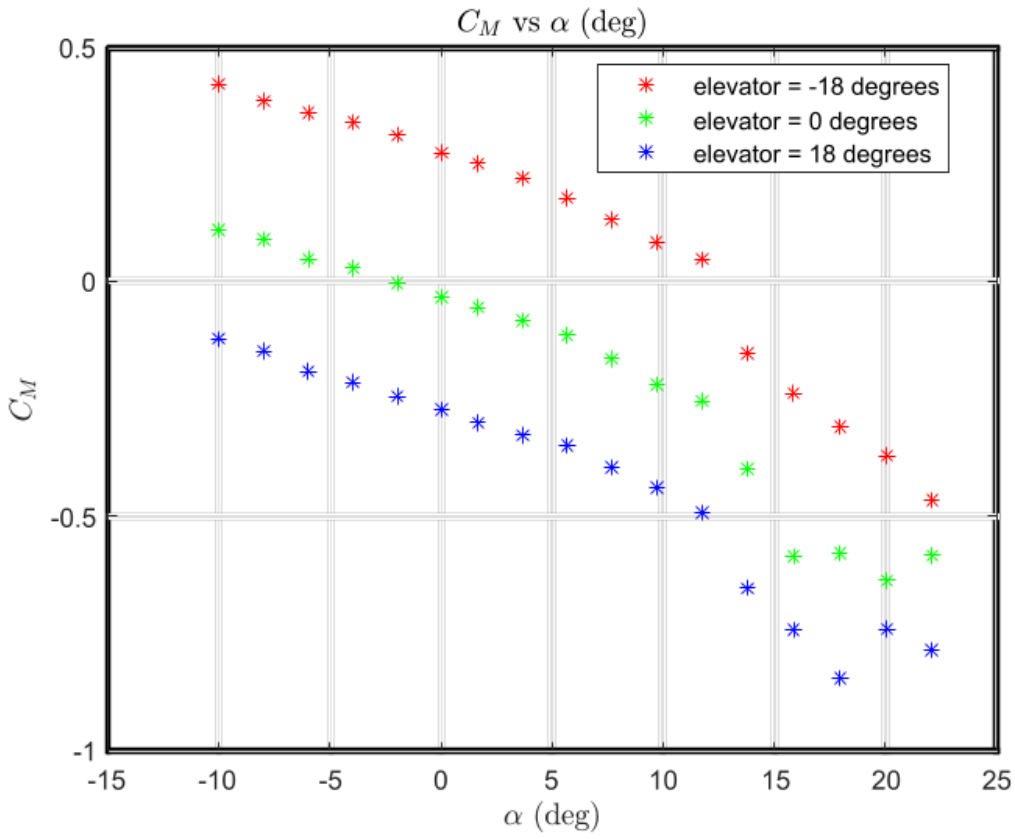

Figure 7: Plot of C_M versus α for all three elevator angles. Note that the y-intercept for 18° and 0° elevator deflection is negative.